RSC Advances

PAPER

View Article Online
View Journal | View Issue

Cite this: *RSC Adv.*, 2019, **9**, 40727

Hydrothermal synthesis and characterization of nanostructured titanium monoxide films

Arūnas Jagminas, *[a] Simonas Ramanavičius, [a] Vitalija Jasulaitiene[a] and Mantas Šimėnas [b]

At the present time, the formation of titanium monoxide (TiO_x) two dimensional (2D) species with distinct composition, size, shape, and a significantly reduced bandgap (E_g) value compared to TiO_2 is of great scientific and practical importance. This paper describes our findings investigating Ti surface oxidation for the formation of TiO_x films possessing a densely-packed nanoplatelet morphology and a low bandgap value. This goal was herein achieved by the hydrothermal treatment of the Ti surface in selenious acid solution kept at a slightly alkaline pH. Furthermore, the nanoplatelet design not typical for TiO_2 porous films was created by this method for the first time. The formation of titanium monoxide, particularly $TiO_{0.84}$, as a major crystalline phase, was verified by XRD and confirmed by EPR investigations. It is worth noting that these nanoplatelet-shaped films with a thickness of 0.1–0.25 μm exhibited a very large shift of their light absorption threshold, down to 1.29 eV, compared to the E_g of anatase TiO_2 and a surprising 70% porosity determined *via* simulation of experimental reflection plots. It is anticipated that this unique TiO_x nanomaterial will pave the way for new investigations and applications.

Received 16th October 2019
Accepted 2nd December 2019

DOI: 10.1039/c9ra08463k

rsc.li/rsc-advances

Introduction

Titanium dioxide, TiO_2, belongs to the group of materials that were most intensely investigated during the past three decades due to their unique optical, dielectric, catalytic properties, chemical resistance, mechanical hardness, nontoxicity and simple processing at a low cost. The crystalline forms of TiO_2-anatase, TiO_2-rutile and TiO_2-brookite polymorphs are well documented. Nanostructured anatase and rutile crystallites possess excellent optical absorption performance under UV light illumination due to their bandgap values of 3.2 eV and 3.06 eV, respectively. They are successfully used in the modern photocatalysis, solar cell devices,[1–3] gas sensors,[4,5] and protective and multilayered coatings.[6] To tune the absorption edge of TiO_2 in the visible light region, the doping of titania with various elements both in the Ti and O sublattice positions has been proposed and discussed in numerous papers.[7–13] Besides, the hybridization of titania with lower bandgap semiconductor nanoparticles and quantum dots, such as Cu_2O,[14] $CuSe_x$,[15] CdSe,[16] *etc.* has been proposed.

Nonstoichiometric semiconducting titanium oxides, namely titanium suboxides, containing structural vacancies in both titanium and oxygen sublattices with a general formula Ti_nO_{2n-1}, where $n \geq 2$, represent a group of less known low band gap materials, well reviewed in the recent years by the Chen[17] and Xu[18] groups. The experimental results have shown that the n value usually varies between 3 and 10,[6] although significantly higher n values were also reported.[19–21] The excellent electric conductivity, and visible light absorption are also characteristic features of titanium monoxides, TiO_x ($x < 2$), making them very suitable for prospective applications in electronic and opto-electronic devices, photo catalysis, batteries, *etc.* For example, the presence of vacancies in $TiO_{1.0}$ results in an $E_g \cong 2.0$ eV, as reported by Gusev.[22] To date different precursors and synthesis methods have been reported for Ti_nO_{2n-1} and TiO_x fabrication.[23–28] From these reports, titanium monoxides can be synthesized from raw TiO_2 powders by high temperature reduction with hydrogen,[23,24] carbon[25,26] and active metals such as Ti, Na, Ca, Mg, Al, and Ca.[27,28] For example, well-mixed probes of TiO_2 and Ti powders can be converted to titanium monoxides *via* arc melting in an oxygen-free atmosphere at 2273 K, and in a tube furnace at 1173 K.[28] Various titanium monoxides have also been synthesized by heating of TiO_2 powders with $CaCl_2$ at 1373 K (ref. 25) and CaH_2 at 625 K.[26] Geng *et al.* established the nanotube-shaped Ti_nO_{2n-1} films by Ti anodizing in the H_2 atmosphere at 1323 K (ref. 29) whereas He *et al.* formed magneli phase Ti_8O_{15} nanowires with a diameter of 30 nm and a length of 2.5 μm on a cleaned Ti substrate by heating together with TiO_2 powders placed separately in a tube furnace under a N_2 stream at 1323 K.[30] However, it is commonly accepted that Ti_nO_{2n-1} is difficult to synthesize. Firstly, processing in the oxygen-free atmosphere at high temperature is required. Secondly, Ti_nO_{2n-1} is unstable even at 425–525 °C temperatures decomposing to various superstructures.[31] As a result, Ti_nO_{2n-1}

[a]State Research Institute Centre for Physical Sciences and Technology, Sauletekio Ave. 3, LT-10257 Vilnius, Lithuania. E-mail: arunas.jagminas@ftmc.lt
[b]Faculty of Physics, Vilnius University, Sauletekio Ave. 9, LT-10222 Vilnius, Lithuania

materials synthesized by heating a mixture of powdered Ti and TiO_2 at high temperature, usually comprised a two-phase composition. To overcome this problem, chemical,[32] electrochemical,[33] mechano-chemical,[34] and flame[35] synthesis methods of Ti_nO_{2n-1} compounds have been proposed.

Here we present a facile synthesis pathway of novel, nanoplatelet-shaped titanium monoxide film on a Ti substrate. It is worth noting that to date there are no reports of the direct formation of titanium monoxide nanoplatelet films well attached to a conductive substrate. The surprising result was obtained in this study *via* hydrothermal oxidation of a titanium substrate in a slightly alkaline selenious acid solution at a quite low temperature, *ca.* 150° to 180 °C. To explain the low bandgap value of titania films with a novel design, EPR investigations were performed.

Materials and methods

Materials

All of the materials were purchased from Sigma-Aldrich unless stated otherwise. Ti foil, 99.7 at% purity and 0.127 mm thick, purchased from Aldrich, was used to prepare specimens of 12 × 12 mm^2. For the EPR investigations, sub-micrometer-sized Ti particles (<20 μm, 93% in water) were purchased from Alfa Aesar.

Synthesis

The surface of Ti samples and particles was ultrasonically cleaned in acetone, ethanol, and water, for 6 min in each, etched in the solution containing H_2O, HNO_3 and HF (20%) (5 : 4 : 1 by volume) at room temperature (RT) for 10 s, well rinsed and air-dried. Nanoplatelet-shaped films on the Ti surface were synthesized as follows. At first, the pH of an aqueous solution containing 0.05 to 0.5 mol L^{-1} of selenious acid (the highest purity, purchased from Russia) was shifted to the alkaline region by dropwise addition of 0.1 mol L^{-1} NaOH solution and intense mixing. Then 15 mL of this solution was poured into a Teflon line stainless steel autoclave of 25 mL volume. Every Ti specimen was mounted vertically in the solution by means of a Teflon holder. For the EPR investigations, the sub-micrometer-sized Ti particles instead of Ti foil specimens were used. The synthesis was conducted at 180° for up to 48 h using a 10 °C min^{-1} ramp. Finally, the products were carefully rinsed with distilled water and dried in air naturally. The annealing of samples was carried out in air and oxygen-free (quartz ampule with Cu foil) atmospheres at 300, 400, and 440 °C for 2 h.

Characterization

The morphology and elemental composition of the obtained products were investigated using scanning electron microscopy FEI Quatra 200F and the Cross Beam Workstation Auriga equipped with the field emission gun and an EDX spectrometer.

X-ray powder diffraction experiments were performed with a D8 diffractometer (Bruker AXS, Germany), equipped with a Göbel mirror as a primary beam monochromator for CuK_α radiation. Diffuse reflectance spectra of titania films were obtained by means of a Shimadzu UV-VIS-NIR spectrophotometer UV-3600 coupled with a MRC-3100 unit. Measurements were performed by mounting a sample holder onto the integrating sphere. The measurable range of wavelengths falls between 200 nm and 850 nm, covering the UV and visible light regions. In the integrating sphere, one beam strikes the sample normally to the surface while the other beam – aslant. The light absorbance was calculated from the diffuse reflection coefficient using the Kubelka–Munk function. X-ray photo electron spectroscopy (XPS) measurements were carried out using the ESCALAB MKII spectrometer equipped with a new XR4 twin anode. The non-monochromatic MgK_α, X-ray source was operated at $h\nu = 1253.6$ eV with 300 W power (20 mA/15 kV) and the pressure in the analysis chamber was lower than 5×10^{-7} Pa during spectral acquisition. The spectra were obtained using an electron analyzer with a pass energy of 20 eV for narrow scans and a resolution of 0.05 eV and with a pass energy of 100 eV for survey spectra. All spectra were recorded at a 90° take-off angle and calibrated using the C 1s peak at 284.6 eV. The spectra calibration, processing and fitting routines were done using the Advantage software (5.918) provided by Thermo VG Scientific. Core level peaks of Ti 2p, Se 3d, and O 1s were analyzed using the nonlinear Shirley-type background and the calculation of the elemental composition was performed on the basis of Scofield's relative sensitivity factors. To investigate the optical properties of titania films, the reflectance spectra of the samples were recorded in the wavelength range of 200–1700 nm using a Shimadzu UV-VIS-NIR spectrophotometer equipped with a MPC-3100 integrating sphere. The specular reflectance of the light from the film surface was calculated using an optical model of two layers. The Bruggeman Effective Medium Approximation (EMA) was applied to calculate the optical constants of the nanoplatelet titanium monoxide film formed on the Ti substrate and consisting of the naturally formed thin layer of TiO_2 and the nanoplatelet titanium monoxide layer with the empty voids (see Scheme 1 in Fig. 6). The porosity of films was calculated by fitting the model functions to the measured data using a CompleteEASE software program, as in our previous study of porous alumina.[36]

EPR investigations

Continuous-wave electron paramagnetic resonance (CW EPR) experiments were performed using a Bruker X-band ELEXSYS E580 EPR spectrometer. The strength and frequency of the modulating field were 0.3 mT and 100 kHz, respectively. Simulations of the CW EPR spectra were performed using EasySpin 5.2.20.[37]

Results and discussion

Selenious acid (H_2SeO_3) aqueous solutions were selected herein due to their known oxidant reactivity[36] through the reaction: $H_2SeO_3 + H_2O + 4e \rightarrow Se^0 + 4OH^-$, resulting in the subsequent oxidation of titanium and the formation of a pale yellow colored film. The annealing in the air as well as in an oxygen free

ampoule at temperatures from 300° to 450 °C for several hours resulted in an obviously darker yellow coloring. Moreover, after calcination of such films at up to 450 °C for 3 h, no obvious changes in the film morphology were detected by SEM.

Our initial investigations revealed that the expected oxidative behavior of the selenious acid towards the Ti substrate under hydrothermal conditions proceed in the 50 to 500 mmol L^{-1} concentration range at the pH of 8 to 11 and at 140–190 °C temperatures. However, uniformly designed nanostructured films were formed mainly in the 0.1–0.3 mol L^{-1} solutions at pH of 9. For evidence, Fig. 1 depicts the top-side SEM images of the Ti surface after autoclaving in 0.2 mol L^{-1} H_2SeO_3 solutions, kept at the pHs of 9.0 and 10.0 at 150° and 180 °C for 15 h. As seen, just at a pH close to 9.0 the films with a novel nanoplatelet-shaped design were formed (Fig. 1a–d). More detailed investigations of these films with a SEM revealed the formation of an array from densely packed nanoplatelets of the length of 80–100 nm and the thickness of 5–12 nm (see Fig. 1b and d), depending on the pH, synthesis temperature and the processing time. It was determined that apart from the pH, the crucial role on the titania film design and the film thickness is played the autoclaving temperature. By increasing the treatment temperature from 150° to 180 °C, the average thickness of the titania layer is increased from about 80–86 nm to 240–260 nm (see insets in Fig. 1).

Under the optimized synthesis conditions (150–180 °C, 15 h), most probably due to the small thickness, the elemental composition of these films cannot be determined by the EDX analysis. X-ray photoelectron spectroscopy (XPS) analysis indicated that the as-formed films on the surface side were mainly composed of titanium and oxygen. Just a small content of selenium was detected by XPS at the film surface. An increase in the concentration of selenious acid from 0.05 to 0.5 mol L^{-1} resulted in the incorporation of just somewhat larger amount of selenium. Noteworthy, at pH of 10.0 (Fig. 1f), there is an obvious difference of the as-formed film morphology because the somotoid-shaped species randomly distributing on the surface are formed. Fig. 2 depicts XRD patterns of the as-formed (a) and annealed (b) film formed on the Ti substrate by hydrothermal treatment in the H_2SeO_3 solution. It can be noted that the as-formed films in the low-concentrated solution, *e.g.* 0.05–0.1 mol L^{-1} for up to 30 h, were found to be composed mainly of amorphous components. In more concentrated H_2SeO_3 solutions, *e.g.* 0.2–0.5 mol L^{-1}, as-formed films were also found to be amorphous but containing titanium monoxide $TiO_{0.84}$ crystallites due to the clearly resolved peak at 2θ 36.92°, corresponding to the peak from the {111} plane. After annealing in the oxygen-containing atmosphere these nanoplatelet films seem to be composed of both crystalline TiO_2 and nonstoichiometric titania phases (see b pattern and inset in Fig. 2). It is reasonable to note that the shift of the main XRD peak ascribed to anatase and usually seen at $2\theta = 25.2°$ to the lower angles, namely 22.6°, could be related to the formation of nonstoichiometric titania. All other experiments, performed without H_2SeO_3 at the varying pH and temperature, have never shown such morphology and the TiO_x phase formation. Furthermore, no detectable peaks corresponding to Se–O or Ti–Se compounds were observed in the XRD patterns of nanoplatelet films formed in the solutions containing from 0.05 to 0.5 mol L^{-1} of H_2SeO_3 by the hydrothermal treatment at the temperatures from 150° to 180 °C for up to 48 h.

To further explore the composition of nanoplatelet-shaped films as-formed by the hydrothermal treatment under the optimized conditions of this study and after calcination at various temperatures, investigation were conducted using CW EPR of the sub-micrometer-sized titanium particles. It is worth noticing, that in this case the quite similar morphology films were formed. Note that EPR is a precise tool to reveal the existence of Ti^{3+} and oxygen vacancies in the titania materials.[38–40] Fig. 3 depicts the EPR spectrum recorded at 110 K for titanium species after hydrothermal treatments in the selenious acid solutions and subsequent calcination in the oxygen-free atmosphere. The spectrum consists of two slightly overlapping signals exhibiting different saturation behavior. The narrow line at $g = 2.0023 \pm 0.0001$ might be attributed to the conduction electrons as previously observed in anatase after thermal reduction at high temperature.[41] We also cannot rule out that the origin of this signal is some free radicals formed during the sample preparation. The second signal is much broader with an effective *g*-value of 1.961 ± 0.003, which is typical for Ti^{3+} ions in various environments and polymorphs of titania.[38,40,41]

X-ray photoelectron spectroscopy (XPS) investigations were carried out to determine the composition and valence states of elements involved in the nanoplatelets. In the survey spectrum (Fig. 4a), the elements of Ti, Se, and O are clearly identified. Besides the above elements, the C element was also observed most probably due to the adventitious hydrocarbon from the XPS spectrometer itself and was not further analyzed. The Ti $2p_{3/2}$ peak (Fig. 4b) can be decomposed into two components centered at 459.6 and 458.5 eV, attributable to different oxidation states of titanium.[42–45] The main component at 458.5 eV corresponds to the Ti^{4+} state.[43–45] The second component at 459.6 eV probably is due to the small or Ti–OH contribution.[43,44] The absence of clearly resolved Ti^{3+} $2p_{3/2}$ binding energy in a vicinity of 456.8–457.8 eV (ref. 46 and 47) most probably should be ascribed to the formation of titanium monoxide mainly in a lower part of film not capable analyze by XPS.

Fig. 4 panel c depicts the high-resolution scans of the Se 3d electrons for the sample obtained by the hydrothermal treatment in the same H_2SeO_3 solutions under the same synthesis conditions, *e.g.* 150 °C for 15 h. From the deconvoluted peak areas, Se is mainly present in the Se^0.[46,47] Furthermore, the incorporation of selenium was estimated to be just ~0.48, ~0.67 and ~1.1 at% for 0.1, 0.3, and 0.5 mol L^{-1} solutions. Besides, the quantity of Se^0 increased with the solution concentration increase from ~28% (at 0.1 mol L^{-1}) to ~33% (at 0.3 mol L^{-1}) and ~83% (at 0.5 mol L^{-1}). In addition, we have found that post-calcination of the nanoplatelet film in the oxygen-free ampoule at 350 °C results in the evaporation of elemental selenium from the titanium monoxide film sublimating onto the walls of the glass tube by drops, well confirming the incorporation of a-Se^0 species instead of formation the titanium selenides.

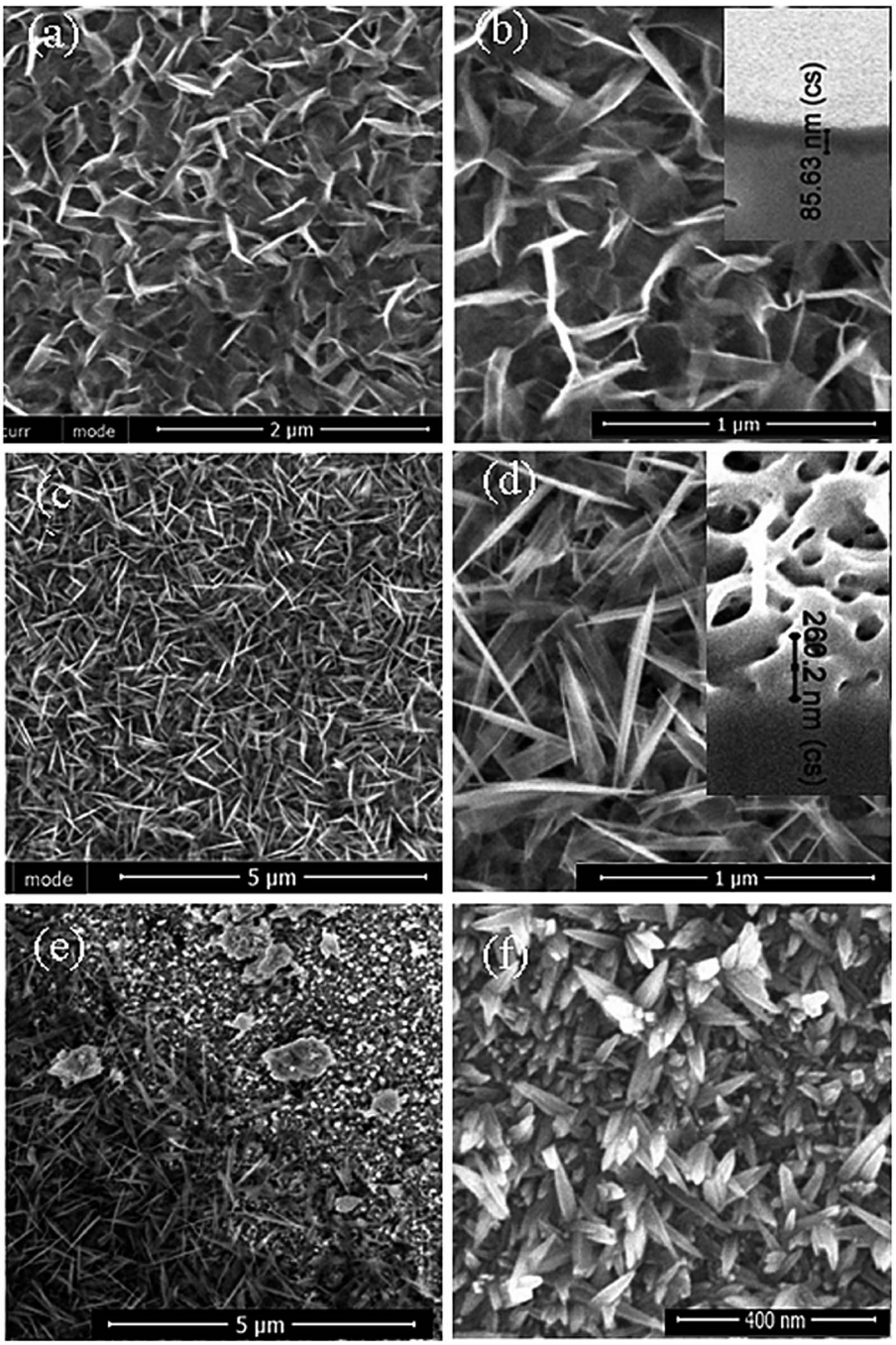

Fig. 1 Top-side FESEM images of the TiO_x film formed on the Ti surface by hydrothermal treatment in the solution containing 0.2 mol L^{-1} H_2SeO_3 and NaOH up to pH = 9.0 (a–e) or pH = 10.0 (f) at 150 °C (a, b and f), 180 °C (c and d) or 200 °C (e) for 15 h. In the insets, the cross-sectional fragments of the corresponding film are presented.

To determine the absorption coefficient and an indirect band gap characteristic of titania films, the diffuse reflectance spectra were further collected and analyzed. The absorption coefficient (A) was calculated by the formula: $A = (1 - R)^2/2R$,[48] where R is the reflectance. The Kubelka Munk function plots for possible indirect transitions [$(Ah\nu)^{1/2}$ *vs.* $h\nu$] of selected nanoplatelet films fabricated under conditions of this study as a function of the subsequent annealing treatments are displayed in Fig. 5. As shown, the film synthesized at 150 °C and annealed in the oxygen-free atmosphere at 350°, 400°, and 440 °C exhibits the optical gap of 2.83, 1.74, and 2.32 eV, respectively. The strongest absorption in the visible range shows the film calcined at 400 °C. With the further T_{an} increase to 440 °C, the E_g value decreased to 2.32 eV, which is significantly lower than a typical E_g value of anatase TiO_2 equal to ~3.2 eV. This result can be ascribed to decomposition of titanium suboxides at $T_{an} \geq 450$ °C, as reported in ref. 49. It is worth noticing that in case of annealing the 180 °C film in the

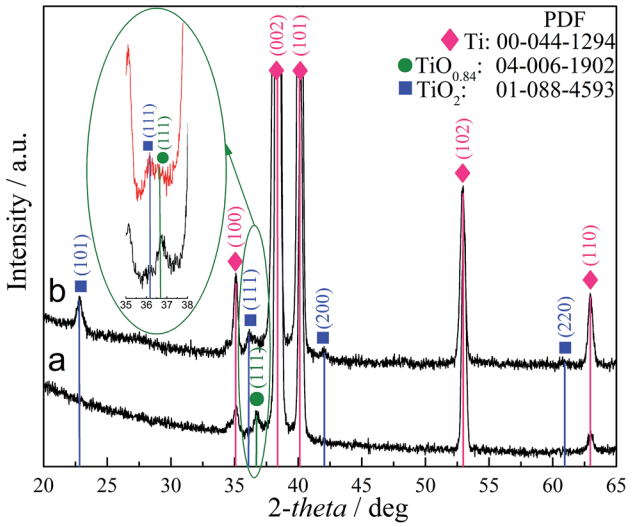

Fig. 2 XRD patterns of the film formed at the Ti substrate by hydrothermal treatment in the solution of 0.2 mol L^{-1} H_2SeO_3 (pH = 9.0) at 150 °C for 15 h before (a) and after (b) annealing in oxygen-containing atmosphere at 350 °C for 2 h.

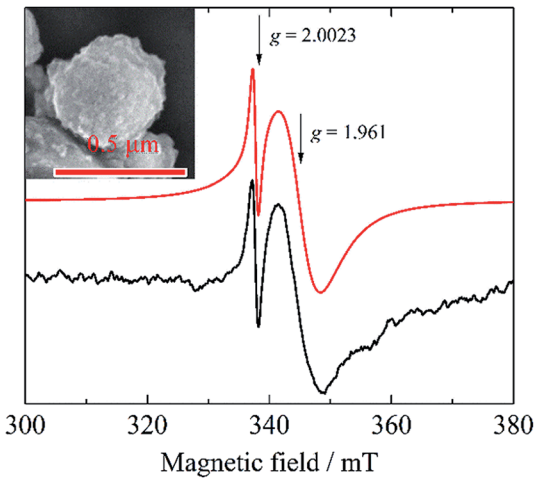

Fig. 3 Experimental (black) and simulated (red) CW EPR spectrum of titanium particles hydrothermally treated in the solution of 0.2 mol L^{-1} selenious acid at 180 °C for 45 h. In the inset, SEM image of $TiO_{0.84}$ coated NP.

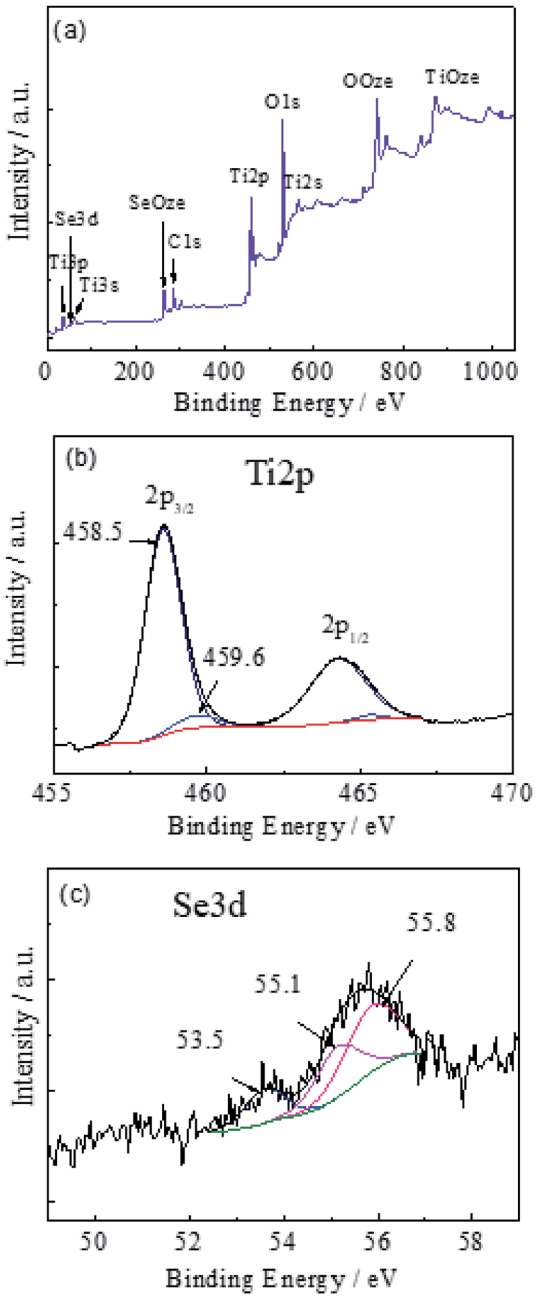

Fig. 4 Survey (a) and deconvoluted X-rays photoelectron spectra of Ti 2p (b) and Se 3d (c) elements encased at the surface side of the film formed on the Ti substrate by hydrothermal treatment in 0.3 mol L^{-1} H_2SeO_3 solution (pH = 9.0) at 150 °C for 15 h.

oxygen-free atmosphere at 400 °C the film possessing the smallest band gap value of 1.29 eV (Fig. 5b) was fabricated.

To determine the possible parameters of the nanoplatelet $TiO_{0.84}$ film formed in the adapted herein solution under the optimized hydrothermal treatment conditions, *e.g.* 180 °C, 15 h, before and after annealing at 400 °C in the air and in the oxygen-free atmosphere, the model of the nanoporous titania film as in ref. 50 and 51 was developed (Fig. 6a) and analyzed. For example, Fig. 6b depicts the experimental reflection *versus* wavelength, $R_p(\lambda)$, plot for the nanoplatelet film calcined in the oxygen-free atmosphere. The same plot was calculated on the basis of the film model and it is presented by a red line. In this way, it was determined that the shape of the theoretically calculated plot $R_p(\lambda)$ well resembled the experimental one if the film thickness approximated 86.6 nm and the surprising 79% porosity well complying with the film structure observation by SEM presented in Fig. 1d.

It can be inferred that an increase in the band gap reduction of nanoplatelet titania could be attributed to the doping with selenium. However, the selenium content in the film is very low, not detectable by XRD and Raman (the data are not presented) and it decreases further upon calcination in the ampoule due to evaporation and sublimation of Se^0 ruling out the possibility to

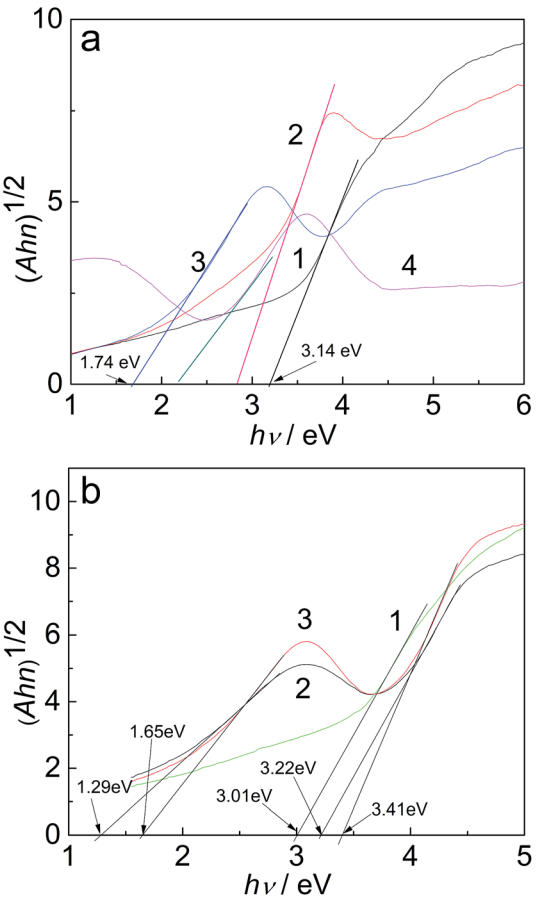

Fig. 5 (a) Tauc plots for indirect transitions of titanium monoxide nanoplatelet arrays formed by hydrothermal treatment in the 0.3 mol L^{-1} H_2SeO_3 solution (pH = 9.0) at 150 °C for 15 h after calcination in the air (1) and oxygen-free atmosphere at: 350 (2); 400 (3), and 440 °C (4) for 2 h. In (b), the same plots for the film grown at 180 °C for 15 h after calcination in air (1) and oxygen-free atmosphere at 400 °C (2) and 440 °C (3) for 2 h.

increase the band gap redshift. To check the influence of Se^0 incorporation, the nanotubed titania (TiNt) films decorated with Se^0 nanoparticles were further designed and their optical properties were investigated. For this purpose, Ti specimens were anodized in the ethylene glycol solution containing NH_4F and H_2O at 50 V for 30 min as previously reported[14] and calcined in the air at 450 °C for 2 h. In this way, the nanotube shaped (Fig. 7a) film of the 4.7 μm thickness with 120 nm tubes at the metal|film interface was formed. For crystallization, the samples were annealed at 450 °C in the air for 2 h ($\partial T/\partial t$ = 10 °C min^{-1}). The decoration of this film with Se^0 was carried out by electrodeposition from the 0.2 mol L^{-1} H_2SeO_3 solution as in the case of alumina.[52] As seen from the Se mapping image (Fig. 7b) and the Se distribution in the film cross-section (Fig. 7c), the adapted herein treatment conditions result in the rather uniform deposition of selenium species throught all the film thickness. Furthermore, the Raman spectra (Fig. 7d) revealed deposition of pure Se^0 species, whereas the XRD pattern (not shown herein) indicated their amorphous nature. Eventually, the diffuse reflectance spectra for several films with various Se^0 contents were investigated and characteristic plots (Fig. 7e) were analyzed. As can be seen, the heterostructuring of titania nanotubes with a-Se species only slightly redshifts the band gap of anatase TiO_2. These results well comply with the reported ones.[53] Therefore, a significant E_g redshift of our nanoplatelet films should be mainly ascribed to the formation of the low band gap titanium monoxide family member $TiO_{0.84}$ confirmed by XRD and EPR.

Conclusions

Herein we demonstrated a simple possibility of forming a low band gap nanoplatelet species array on a Ti substrate by hydrothermal synthesis and a subsequent calcination. For this purpose, selenious acid solutions kept at a pH close to 9.0 were successfully used for the first time. The current study shows that the nanoplatelet shaped film, of a thickness up to 250 nm formed under the optimized hydrothermal treatment conditions of this study, is mainly composed of semiconducting titanium monoxide $TiO_{0.84}$ with an indirect optical band gap value as low as 1.29 eV. The nanotube-shaped anatase TiO_2 film decorated with Se^0 species was

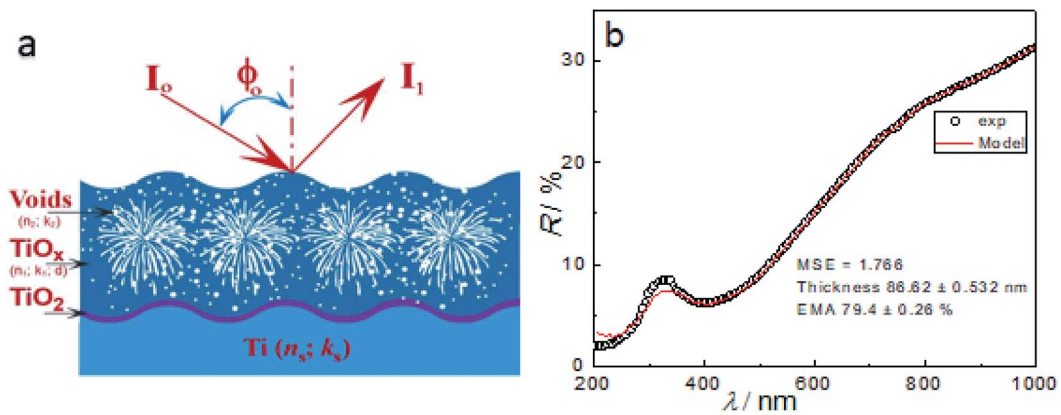

Fig. 6 (a) The scheme corresponding to the model used for the fitting of experimental $R(\lambda)$ dependency. In (b) the reflection *vs.* wavenumber (λ) plots for experimental 180 °C $TiO_{0.84}$ film (circles) and the calculated one (line) by the adapted nanoporous film model.

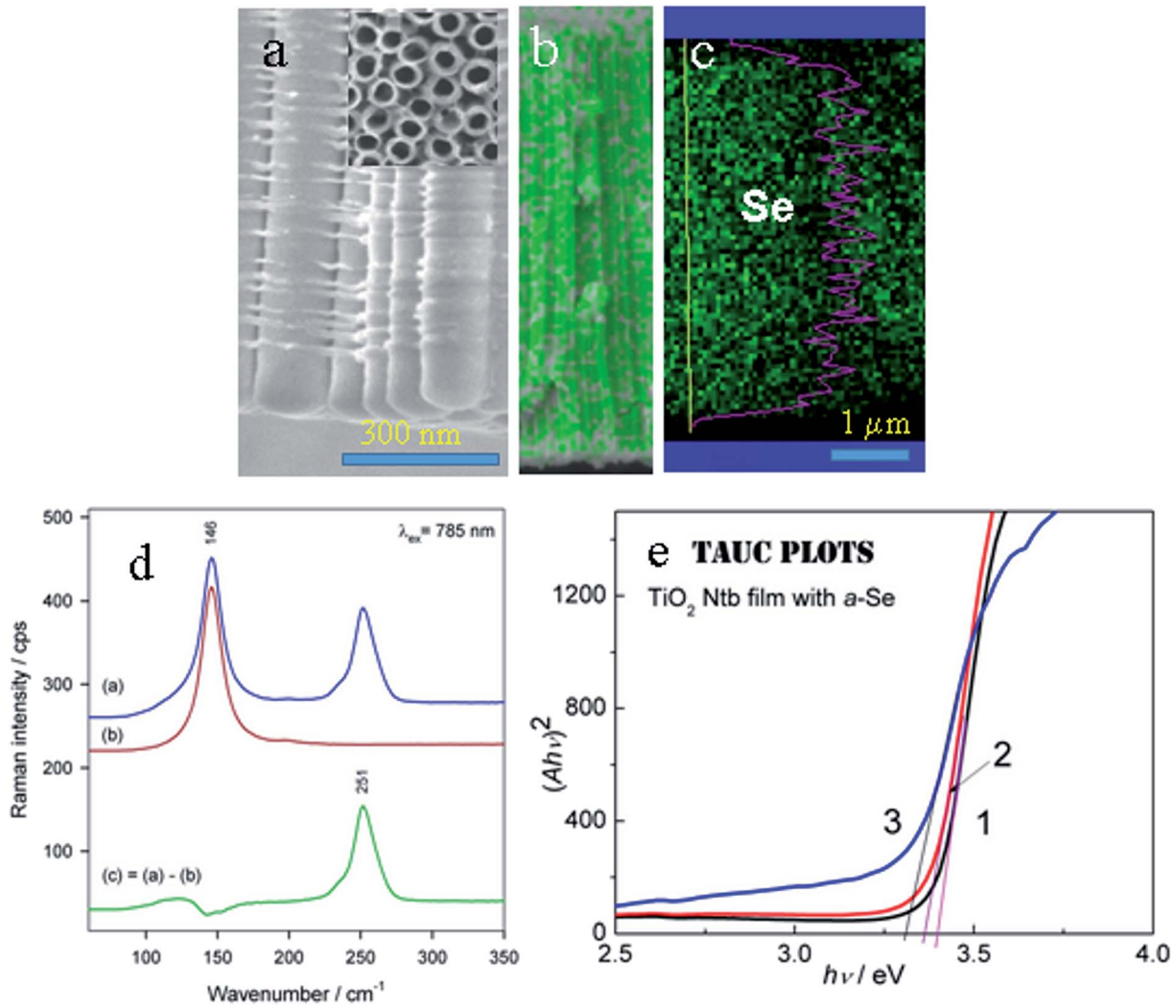

Fig. 7 Panoramic (a), top-side (inset), and cross-sectional (b) SEM views of anatase TiO_2 film fabricated by Ti anodizing in the ethylene glycol solution containing 0.25 NH_4F and 1.0 wt% H_2O at 50 V for 30 min followed by calcination at 450 °C for 2 h before (a) and after the Se DC deposition in 0.005 mol L^{-1} H_2SeO_3 solution at −2.0 V for 5 min (b). In (c) the element map and distribution profile of the Se species encased inside the film across all the TiO_2 film thickness *ca.* 4.75 μm. In (d) the Raman spectra of TiNt/Se (a), pure TiNt (b) and difference (c). In (e) the Tauc plots of TiNt film before (1) and after DC deposition of a-Se at 1.5 V for 2 (2) and 7 (3) min.

also designed and studied herein. The comparison of its optical properties with the those of our film implied that the significant E_g redshift of our nanoplatelet films should be ascribed to the formation of the low band gap titanium monoxide family member $TiO_{0.84}$ confirmed by XRD and EPR. We suppose that these nanotechnology-driven titania films could have an indispensable potential to discover novel sensor devices in the future.

Author contributions

A. J. designed, supervised and managed the study. S. R. performed syntheses and morphological characterization of the products. The XPS, and EPR investigations were carried out by V. J. and M. Š., respectively. All authors have given approval to final version of the manuscript.

Conflicts of interest

The authors declare no competing financial interest and any unpaid roles or relationships that might have a bearing on the publication process.

Acknowledgements

We acknowledge the help of Dr V. Pakštas for collection of XRD patterns, and Mr Arnas Naujokaitis for SEM observations.

References

1 M. Grätzel, Photoelectrochemical cells, *Nature*, 2001, **414**, 338–344.

2 B. O'Regan and M. Grätzel, A low-cost, high-efficiency solar cell based on dye-sensitized colloidal TiO_2 films, *Nature*, 1991, **353**, 737–740.
3 B. S. Richards, S. F. Rowlands, A. Ueranatasun, J. E. Cotter and C. B. Honsberg, Potential cost reduction of buried-contact solar cells through the use of titanium dioxide thin films, *Sol. Energy*, 2004, **76**, 269–276.
4 H. Tang, K. Prasad, R. Sanjinés and F. Lévy, TiO_2 anatase thin films as gas sensors, *Sens. Actuators, B*, 1995, **26**, 71–75.
5 O. K. Varghese, G. K. Mor, C. A. Grimes, M. Paulose and N. Mukherjee, A Titania Nanotube-Array Room-Temperature Sensor for Selective Detection of Hydrogen at Low Concentrations, *J. Nanosci. Nanotechnol.*, 2004, **4**, 733–737.
6 Y. Sawada and Y. Taga, TiO_2/(indium tin oxide) multilayer film: a transparent IR reflector, *Thin Solid Films*, 1984, **116**, L55–L57.
7 K. S. Yeung and Y. W. Lam, A simple chemical vapour deposition method for depositing thin TiO_2 films, *Thin Solid Films*, 1983, **109**, 169–178.
8 M. K. Nazeeruddin, A. Kay, I. Rodicio, R. Humphry-Baker, E. Mueller, P. Liska, N. Vlachopoulos and M. Graetzel, Conversion of light to electricity by cis-X2bis(2,2'-bipyridyl-4,4'-dicarboxylate)ruthenium(II) charge-transfer sensitizers (X = Cl-, Br-, I-, CN-, and SCN-) on nanocrystalline titanium dioxide electrodes, *J. Am. Chem. Soc.*, 1993, **115**, 6382–6390.
9 D. C. Gilmer, D. G. Colombo, C. J. Taylor, J. Roberts, G. Haugstad, S. A. Campbell, H. S. Kim, G. D. Wilk, M. A. Gribelyuk and W. L. Gladfelter, Low temperature CVD of crystalline titanium dioxide films using tetranitratotitanium(IV), *Adv. Mater.*, 1998, **10**, 9–11.
10 K. L. Siefering and G. L. Griffin, Growth Kinetics of CVD TiO_2: Influence of Carrier Gas, *J. Electrochem. Soc.*, 1990, **137**, 1206–1208.
11 J. C. Yu, J. Yu and J. Zhao, Enhanced photocatalytic activity of mesoporous and ordinary TiO_2 thin films by sulfuric acid treatment, *Appl. Catal., B*, 2002, **36**, 31–43.
12 F. Tian and C. Liu, DFT description on electronic structure and optical properties of anionic S-doped anatase-TiO_2, *J. Phys. Chem. B*, 2006, **110**, 17866–17871.
13 C. Burda, Y. B. Lou, X. B. Chen, A. C. S. Samia, J. Stout and J. L. Gole, Enhanced nitrogen doping in TiO_2 nano particles, *Nano Lett.*, 2003, **3**, 1049–1051.
14 A. Jagminas, J. Kovger, A. Rėza, G. Niaura, J. Juodkazyte, A. Selskis, R. Kondrotas, B. Šebeka and J. Vaičiūnienė, Decoration of the TiO_2 nanotube arays with copper suboxide by AC treatment, *Electrochim. Acta*, 2014, **125**, 516–523.
15 A. Jagminas, J. Kovger, A. Selskis and A. Rėza, Effect of hydrogen doping on the loading of titania nanotube films with copper selenide species via alternating current deposition, *J. Appl. Electrochem.*, 2015, **45**, 1141–1151.
16 I. Zerazua, E. De la Rosa, T. Lopez-Luke, J. Reyes-Gomez, S. Ruiz, C. Ageles Chavez and J. Z. Zhang, Photovoltaic Conversion Enhancement of CdSe Quantum Dot-Sensitized TiO_2 Decorated with Au Nanoparticles and P3OT, *J. Phys. Chem. C*, 2013, **115**, 23209–23220.
17 X. Chen, L. Liu and F. Huang, Black titanium dioxide (TiO_2) nanomaterials, *Chem. Soc. Rev.*, 2015, **44**, 1861–1885.
18 B. Xu, H. Y. Sohn and Y. Mahassab, Structures, preparation and applications of titanium suboxides, *RSC Adv.*, 2016, **6**, 79706–79722.
19 P. Waldner and G. Ericson, Thermodynamic modelling of the system titanium-oxygen, *Calphad*, 1999, **23**, 189–218.
20 P. Waldner, Modelling of oxygen solubility in titanium, *Scr. Mater.*, 1999, **40**, 969–974.
21 G. Ericson and A. D. Pelton, Critical evaluation and optimization of the thermodynamic properties and phase diagrams of the MnO-TiO_2, MgO-TiO_2, FeO-TiO_2, Ti_2O_3-TiO_2, Na_2O-TiO_2, and K_2O-TiO_2 systems, *Metall. Mater. Trans. B*, 1993, **24**, 795–805.
22 A. I. Gusev, *Physical Chemistry of Nonstoichiometric Refractory Compounds*, Nauka, Moscow, 1991.
23 M. Radecka, A. Trenczek-Zajac, K. Zakrzewska and M. Rekas, Effect of oxygen nonstoichiometry on photo-electrochemical properties of TiO_{2-x}, *J. Power Sources*, 2007, **173**, 816–821.
24 Y.-W. Lee, H.-D. Kwak, A.-R. Park, B. Roh, I. Hwang, G. Cao and K.-W. Park, Facile and Catalytic Synthesis of Conductive Titanium Suboxides for Enhanced Oxygen Reduction Activity and Stability in Proton Exchange Membrane Fuel Cells, *Int. J. Electrochem. Sci.*, 2013, **8**, 9499–9507.
25 Z. Cao, W. Xie, I.-H. Jung, G. Du and Z. Qiao, Critical Evaluation and Thermodynamic Optimization of the Ti-C-O System and Its Applications to Carbothermic TiO_2 Reduction Process, *Metall. Mater. Trans. B*, 2015, **46**, 1782–1801.
26 M. Toyoda, T. Yano, B. Tryba, S. Mozia, T. Tsumura and M. Inagaki, Preparation of carbon-coated Magneli phases Ti_nO_{2n-1} and their photocatalytic activity under visible light, *Appl. Catal., B*, 2009, **88**, 160–164.
27 C. Hauf, R. Kniep and G. Pfaff, Preparation of Various Titanium Suboxide Powders by Reduction of TiO_2 with Silicon, *J. Mater. Sci.*, 1999, **34**, 1287–1292.
28 A. S. Bolokang, D. E. Motaung, C. J. Arendse and T. F. G. Muller, Morphology and structural development of reduced anatase-TiO_2 by pure Ti powder upon annealing and nitridation: synthesis of TiO_x and TiO_xN_y powders, *Mater. Charact.*, 2015, **100**, 41–49.
29 P. Geng, J. Su, C. Miles, C. Comninellis and G. Chen, *Electrochim. Acta*, 2015, **153**, 316–324.
30 C. He, X. Chang, X. Huang, Q. Wang, A. Mei and P. K. Shen, Direct synthesis of pure single-crystalline magnéli phase Ti_8O_{15} nanowires as conductive carbon-free materials for electrocatalysis, *Nanoscale*, 2015, **7**, 2856–2861.
31 J. L. Murray and H. A. Wriedt, The O-Ti (Oxygen Titanium) System, *Bull. Alloy Phase Diagrams*, 1987, **8**, 148–165.
32 D. S. Shibuta, S. Koboyashi, M. Yoshizumi and H. Arai, *US Pat.* 4668501, 1987.
33 E. Wainer and M. E. Sibert, *US Pat*. 2707168, 1950.

34 I. Velkovic, D. Poleti, M. Zdujic, L. Karavic and C. Jovalekoc, Mechanochemical synthesis of nanocrystalline titanium monoxide, *Mater. Lett.*, 2008, **62**, 2769–2771.

35 A. Teleki and S. E. Pratsinis, Blue nano titania made in diffusion flames, *Phys. Chem. Chem. Phys.*, 2009, **11**, 3742–3747.

36 A. Jagminas, R. Žalnėravičius, A. Rėza, A. Paškevičius and A. Selskienė, Design, optical and antimicrobial properties of extremely thin alumina films colored with silver nanospecies, *Dalton Trans.*, 2015, **44**, 4512–4519.

37 S. Stoll, EasySpin, a comprehensive software package for spectral simulation and analysis in EPR, *J. Magn. Reson.*, 2006, **178**, 42–55.

38 J. M. Coronado, A. J. Maira, J. C. Conesa, K. L. Yeung, V. Augugliaro and J. Soria, EPR study of the surface characteristics of nanostructured TiO_2 under UV irradiation, *Langmuir*, 2001, **17**, 5368–5374.

39 R. F. Howe and M. Grätzel, EPR observation of trapped electrons in colloidal TiO_2, *J. Phys. Chem.*, 1985, **89**, 4495–4499.

40 M. Kus, T. Altantzin, S. Vercauteren, J. Caretti, O. Leenaerts, K. Batenburg, M. Mertens, V. Meynen, B. Partoens, S. V. Doorslaer, S. Bals and P. Cool, Mechanistic Insight into the Photocatalytic Working of Fluorinated Anatase {001} Nanosheets, *J. Phys. Chem.*, 2017, **121**, 26275–26286.

41 A. L. Attwood, D. M. Murphy, J. L. Edwards, T. A. Egerton and R. W. Harrison, An EPR study of thermally and photochemically generated oxygen radicals on hydrated and dehydrated titania surfaces, *Res. Chem. Intermed.*, 2003, **29**, 449–465.

42 V. Jandova, Z. Bastl, J. Šubrt and J. Pola, Infrared laser-produced carbon-phase shield to oxidation of nanosized titanium monoxide, *J. Anal. Appl. Pyrolysis*, 2011, **92**, 287–291.

43 F. Peng, L. Cai, L. Huang, H. Yu and H. Wang, Preparation of nitrogen-doped titanium dioxide with visible-light photocatalytic activity using a facile hydrothermal method, *J. Phys. Chem. Solids*, 2008, **69**, 1657–1664.

44 G. Shu, H. Wang, H.-X. Zhao and X. Zhang, Microwave-assisted synthesis of black titanium monoxide for synergistic tumor phototherapy, *ACS Appl. Mater. Interfaces*, 2019, **11**, 3323–3333.

45 W. Ni, M. Li, J. Cui, Z. Xing, Z. Li, X. Wu, E. Song, M. Gong and W. Zhou, 808 nm light triggered black TiO_2 nanoparticles for killing of bladder cancer cells, *Mater. Sci. Eng., C*, 2017, **81**, 252–260.

46 Y. Cong, J. Zhang, F. Chen and M. Anpo, Synthesis and characterization of nitrogen-doped TiO_2 nanophotocatalyst with high visible light activity, *J. Phys. Chem. C*, 2007, **111**, 6976.

47 N. Gopal, G. Rocker and R. Feierabend, Intrinsic defects of TiO_2 (110): Interaction with chemisorbed O_2, H_2, CO and CO_2, *Phys. Rev. B: Condens. Matter Mater. Phys.*, 1983, **28**, 3427.

48 V. Štengl, S. Bakardjieva and J. Bludska, Se and Te-modified titania for photocatalytic applications, *J. Mater. Sci.*, 2011, **46**, 3523–3536.

49 S. Lee and C. Jeon, Fabrication of TiO_2 tubules by template synthesis and hydrolysis with water vapor, *Chem. Mater.*, 2004, **16**, 4292–4297.

50 P. Simon, B. Pignon, B. Miao, S. Coste-Leconte, S. Leconte, Y. Marguet, P. Jegou, B. Bouchet-Fabre, C. Reynaud and N. Herlin-Boime, N-doped titanium monoxide nanoparticles with TiO rock-salt structure, low energy band gap, and visible light activity, *Chem. Mater.*, 2010, **22**, 3704–3711.

51 N. Ghrairi and M. Bouaicha, Structural, morphological and optical properties of TiO_2 films by the electrophoretic deposition technique, *Nanoscale Res. Lett.*, 2012, **7**, 357.

52 A. Jagminas, R. Žalnėravičius, R. Rėza, A. Paškevičius and A. Sielskienė, Design, optical and antimicrobial properties of extremely thin alumina films colored with silver nanospecies, *Dalton Trans.*, 2015, **44**, 4512–4519.

53 A. Jagminas, I. Gailiūtė, G. Niaura and R. Giraitis, Template-assisted fabrication of pure Se nanocrystals in controllable dimensions, *Chemija*, 2005, **16**, 15–20.